Correlation-induced emergent charge order in metallic vanadium dioxide

Christopher N. Singh [1,*] L. F. J. Piper [1,*] Hanjong Paik [2] Darrell G. Schlom [2,3] and Wei-Cheng Lee [1,†]
[1]*Department of Physics, Applied Physics, and Astronomy, Binghamton University, Binghamton, New York 13902, USA*
[2]*Department of Materials Science and Engineering, Cornell University, Ithaca, New York 14853-1501, USA*
[3]*Kavli Institute at Cornell for Nanoscale Science, Ithaca, New York 14853, USA*

(Received 7 May 2020; revised 13 January 2022; accepted 18 January 2022; published 31 January 2022)

Recent progress in the growth and characterization of thin-film VO_2 has shown its electronic properties can be significantly modulated by epitaxial matching. To throw new light on the concept of "Mott engineering," we develop a symmetry-consistent approach to treat structural distortions and electronic correlations in epitaxial VO_2 films under strain, and compare our design with direct experimental probes. We find strong evidence for the emergence of correlation-driven charge order deep in the metallic phase, and our results indicate that exotic phases of VO_2 can be controlled with epitaxial stabilization.

DOI: 10.1103/PhysRevB.105.035150

I. INTRODUCTION

The nature of the metal-insulator transition (MIT) in VO_2 has far reaching implications for both fundamental physics [1–4] and blossoming applications in neuromorphic computing [5–9]. From a fundamental viewpoint, the correlation effects of 3*d* orbitals in transition metal oxides exhibit rich ground-state properties ranging all the way from metallic ferromagnets to wide-gap semi-conductors [10,11]. For instance, the MIT in VO_2 is near room temperature, but the isoelectronic compound NbO_2 has a transition temperature orders of magnitude higher [12,13], and TiO_2 lacks a transition entirely [14]. The origin of the MIT in VO_2 remains contested [15] after years of study because neither a Peierls [10,16,17] nor a Mott picture align entirely with all the experimental evidence [18–24]. The scenario where a Peierls distortion and Mott physics cooperatively lead to the MIT has also been investigated extensively [25–31]. Resolving this issue has become even more pressing with the advent of vanadium-based memristor technologies [32–35] that could exploit Mott transitions for beyond von Neumann computing [36]. While the resistivity switching in these new memristors is achieved by driving in a nonequilibrium thermal environment, disputes remain as to the origin of the switching [37]. This situation has redirected massive experimental efforts towards understanding epitaxial VO_2 thin films using TiO_2 substrates, which offer the possibility of enhancing electron correlation effects with severe strain even before the Peierls distortion [38–44].

TiO_2 is a wide-gap system ($\sim$3.2eV) with a stable rutile crystal structure at all temperatures, making it an excellent substrate for VO_2 thin film engineering. Because the *c*-axis lattice constant of TiO_2 is $\sim$3.8% longer than bulk VO_2, strain effects in epitaxial VO_2 films can be modulated by choosing the growth direction on TiO_2 substrates. It has been observed that if the growth direction is perpendicular to the rutile *c*-axis, e.g., VO_2 [100] and VO_2 [110], the elongation of the *c*-axis of VO_2 due to strain gives rise to stronger correlation effects, resulting in a number of new phases including the intermediate insulating M_2 phase [42], an orbital selective Mott state [41], and the enhancement of the lower Hubbard band [43]. These results demonstrate that VO_2 thin films are a unique platform for "Mott engineering," and can exhibit richer correlation effects not observed in bulk VO_2. However, a theoretical description of the interplay between strain and electron correlation is still far from complete [45]. A definitive theoretical treatment of VO_2 across different thin film growth orientations within a common group representation is necessary to address important questions such as the effects of lattice symmetry breaking on electron-electron correlation, phase diagrams of emerging electron states of matter, and so on. In particular, the theoretical framework has to address how lattice and orbital degrees of freedom are influenced in thin films where geometrical degeneracies are lifted by strain [46–48].

Here we determine the Bravais system that seamlessly connects different strain conditions in VO_2 grown on TiO_2 substrates, and employ density functional theory with appropriate functionals that capture all relevant features of the MIT in VO_2 including the gap, magnetic order, energy hierarchy, and so on [49–51]. With this methodology, we are able to study systematically the evolution of correlation effects under different strains. We show that our first-principles atomistic models reproduce the experimental trends in the O *K*-edge x-ray absorption spectrum (XAS) in VO_2 [001], VO_2 [100], and VO_2 [110]. As XAS is often used to detect charge disproportionation [52,53], we contrast our theory against the experiment and find strong evidence that, in highly strained systems, a novel electronic charge order (CO) emerges in the metallic rutile phase before the structural transition occurs due directly to the interplay between electron-electron correlation and local symmetry breaking arising from strain. This

*csingh5@bighamton.edu
†wlee@binghamton.edu

CO naturally leads to two independent vanadium positions inside the rutile unit cell, paving the way for the occurrence of the M_2 phase observed in previous experiments [42]. Our results demonstrate that strain-engineered VO_2 thin films are a unique correlated system allowing tunable Mott correlation and a rich phase diagram featuring a strongly correlated metal.

II. METHODS

Using TiO_2 as a substrate, there are several possible growth orientations for VO_2 [55]. The growth and measurement techniques employed in this work are detailed in Refs. [39] and [40–42]. Here we will adhere to the standard naming scheme where a Miller index in the rutile basis denotes the common vector between both film and substrate and is normal to the interface. This uniquely defines the considered growth directions ([001], [100], and [110]). Because many first-principles approaches implement symmetry mapping operations to conserve computation, and because we want to cross-compare simulations in different point groups, we determine space group 6 (*Pm*) as the lowest common Bravais lattice for the [001], [100], and [110] films. This ensures that no artificial symmetry is enforced or broken in the simulation while the self-consistency condition is reached. A similar approach was applied in the sister compound NbO_2 to investigate structural effects across a metal-to-insulator transition [56].

The lattice parameters for the [001] and [100] growth orientations can be calculated straightforwardly in the original rutile atomic basis because it is commensurate with the rutile TiO_2 symmetry, however, to simulate the [110] growth condition, a linear map is applied to the VO_2 basis defined by

$$\mathcal{M} = \begin{pmatrix} 1 & 1 & 0 \\ -1 & 1 & 0 \\ 0 & 0 & 1 \end{pmatrix}. \tag{1}$$

This defines the growth direction along the crystallographic *b*-axis as shown in Fig. 1. If the volume of bulk VO_2 is Ω, the growth direction lattice vector of VO_2 can be determined as

$$a_3^{\mathrm{VO_2}} = \frac{\Omega}{a_1^{\mathrm{TiO_2}} \cdot a_2^{\mathrm{TiO_2}}}. \tag{2}$$

In Eq. (2) the numerical subscripts can be permuted as needed to represent the out of plane direction depending on the growth orientation. To determine the new lattice vectors, the same map $\mathcal{M}$ is applied to the TiO_2 lattice vectors, the in-plane vectors are matched, and the out-of-plane vector is determined with Eq. (2). Then the inverse map $\mathcal{M}^{-1}$ is applied. This procedure keeps the atomic basis the same, but may change the lattice vectors and the angles. The experimental film characterization is given in Ref. [42] and the parameters used in the simulation are given in Table I.

The electronic structure simulations were performed within the WIEN2K [57] ecosystem. In the occupation number calculations, a 20 000 *k*-point sampling was used with an RKmax of 7.2. The RMT's were fixed to 1.82 and 1.65 a.u. for vanadium and oxygen, respectively, and the GMAX was set to 14. This is necessary so that the mixed basis sets used in the computation are consistent. Several exchange-correlation functionals are compared including Perdew Burke-Ernzerhof (PBE) [58], modified Becke-Johnson (mBJ) [59], and strongly constrained and appropriately normed (SCAN) [60]. Spin orbit coupling is known to be a negligible energy scale and no magnetic ordering was stabilized.

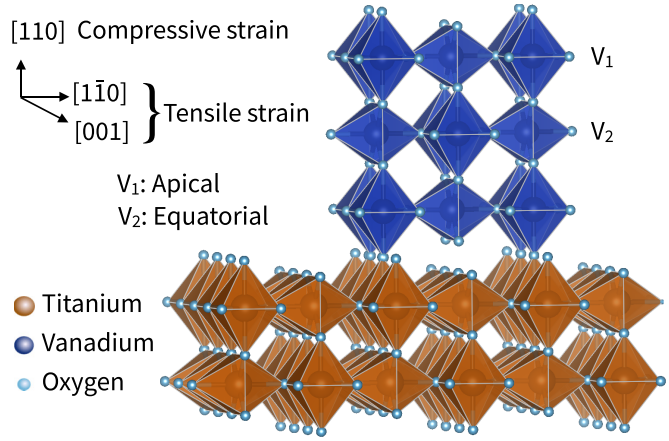

FIG. 1. Rutile VO_2 shown in transformed basis (growth condition). [110] growth affects the two vanadium positions differently by modulating either apical or equatorial bond distances. Image by VESTA [54].

Being that quantum mechanics only defines a continuous charge density distribution, the definition of how much charge is assigned to a specific atom is a subtle question [61] that has been approached in many ways. For example, Mulliken [62], Bader [63], and Hirshfeld [64] all have well-known methods. We choose here the density matrix formalism. In the full-potential-linear-augmented-plane-wave method [65], the Kohn-Sham eigenfunctions $|\psi_i\rangle$ have some components that are atomic-like and can be written as linear combinations of spherical harmonics in the commonly accepted way $|lm\sigma\rangle$. These are defined inside a radial basin of radius R_{MT}. Defining the density matrix as

$$\hat{n}_{lmm'\sigma\sigma'} = \sum_{\varepsilon_i \leqslant \mathrm{E_f}} \langle lm'\sigma'|\psi_i\rangle\langle\psi_i|lm\sigma\rangle, \tag{3}$$

the density of electrons in the *d* level n_d can be calculated by tracing out the orbitals as $\mathrm{Tr}[\hat{n}_d]$. This allows for a quantitatively consistent definition of the radial wave function assigned to each atomic site across all structural phases. In this way, the amount of charge around a given atom is consistently monitored as the strain is applied.

In defining the *d* orbitals, we follow the conventions laid down in the seminal work by Eyert [10]. Because there are

TABLE I. Lattice parameters used in strain simulation.

Parameter	Bulk	[001]	[100]	[110][a]
a (Å)	4.55460	4.59330	4.35141	4.47399
b (Å)	4.55460	4.59330	4.59330	4.47399
c (Å)	2.85140	2.80355	2.95940	2.95940

[a]In this case the monoclinic angle is $\gamma \approx 93.1^\circ$.

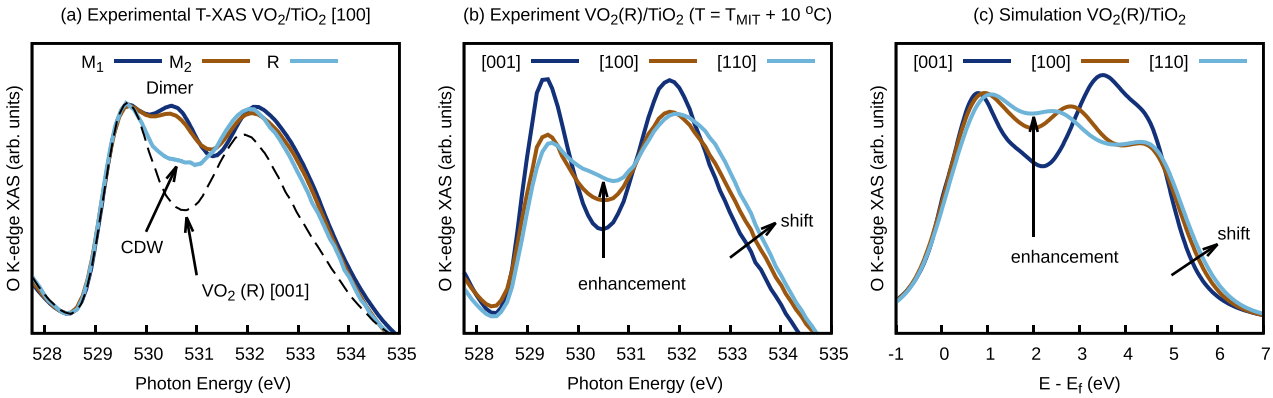

FIG. 2. (a) Strain-induced spectral properties ($E \| c_R$) adapted from Quackenbush *et al.* [42]. The temperature dependence of the oxygen K-edge across the transitions show that dimerization is differentiable from charge/orbital ordering by comparing against VO_2 (R) [001] (dashed line). (b) The enhancement in the peak at ≈530.5 eV compared to the bulk phase is a signature of inequivalent vanadium positions [42], and the corresponding vanadium L-edge has been used to show strain-induced orbital selectivity [43]. The measurement was taken deep inside the metallic state, and yet signatures of vanadium differentiation are observed, providing strong evidence for the onset of correlation stabilized charge order. (c) mBJ level simulation of VO_2(R) oxygen K-edge demonstrating the response of electronic structure to strain results in experimentally observed spectral features.

two different local octahedral environments for vanadium with respect to the global crystallographic system as shown in Fig. 1, the convention is to orient the local coordinate systems such that the z axis points along either the [110] or the [1$\bar{1}$0] directions for V_2 and V_1, respectively. This choice is ensures the d_{xy} and the d_{z^2} orbitals form the e_g manifold and lie higher in energy than the remaining three that form the t_{2g} manifold.

III. RESULTS

The effect on the electronic structure in response to lattice symmetry breaking is found by contrasting the experimental and simulated XAS summarized in Fig. 2. While it is well known that the 530.5 eV peak is enhanced in the M_2 phase relative to the rutile phase [42] and the M_2 phase is known to have two inequivalent vanadium sites, we stress that this is not an observation of the M_2 phase as evidenced by Figs. 2(a) and 3(a). In Fig. 2(b), different growth orientations within the rutile phase (the measurement was performed well above the transition temperature in high quality films) enhance the 530.5 eV spectral feature—a strong fingerprint that vanadium differentiation has developed. One might expect that, since the [110] growth orientation can break the V_1-V_2 equivalency directly, the observed features are simply a result of lattice symmetry breaking, however, as is shown in Fig 3(b), without considering nonlocal correlations, there is no splitting in the spectral function of unoccupied states. This means the spectral weight transfer is a direct result of lattice and correlation interplay that is strongly enhanced in the [110] growth because neither alone can reproduce the experiment. We additionally see similar effects in the [100] growth orientation where explicit lattice symmetry breaking does not occur, but spectral signatures of correlation enhancement persist [43,44]. Ultimately, the evolution of the XAS waveform represents an experimental signature that nonlocal correlations have broken the equivalence between the two vanadium sites in the rutile phase and the spectral features are qualitatively reproduced by a first-principles analysis.

Figure 3(b) shows the density of states for the t_{2g} manifold where it is observed that [110] epitaxial growth modifies the $d \cdot p$ orbital hybridization differently for V_1 and V_2. For the octohedra oriented along the growth direction, the apical bond distance is shortened. For V_1, the d_{xz} orbital lies along this compressed axis, increasing the hybridization as pushing the energy higher. The opposite effect is seen for V_2, where because the d_{xz} is rotated 90° about the rutile c-axis, the hybridization is decreased relative to the unstrained sample, ultimately lowering the onsite energy. For the other four d orbitals, the V_1 spectral function is lowered, while the V_2 spectral function is raised in energy. The high-energy e_g manifold is not shown because the weight at the chemical potential of these orbitals is small. One can see, however, that even in the strained case, the t_{2g} weight at the Fermi level is roughly equal for each vanadium at the generalized gradient approximation (GGA) level. However, with a functional that correctly predicts every other facet of VO_2 such as mBJ [49], we find charge order developing in the low-lying manifold, and the only assumption we drop that others have made is that V_1 is strictly equivalent to V_2 in strained metallic samples. This redistribution of spectral weight has the additional consequence of modulating orbital occupation as shown in Fig. 3(c), where we show that another semi-local approximation containing a kinetic energy density term such as SCAN enhances the difference between the two vanadium sites. We conclude that even though symmetry breaking can occur at the level of the lattice, the electron-ion dynamics in VO_2 are deeply intertwined, and also that correlation effects can stabilize a previously undiscovered charge order in metallic VO_2.

IV. DISCUSSION

Our theoretical and experimental results support the cooperative scenario for VO_2 that both structural distortion and

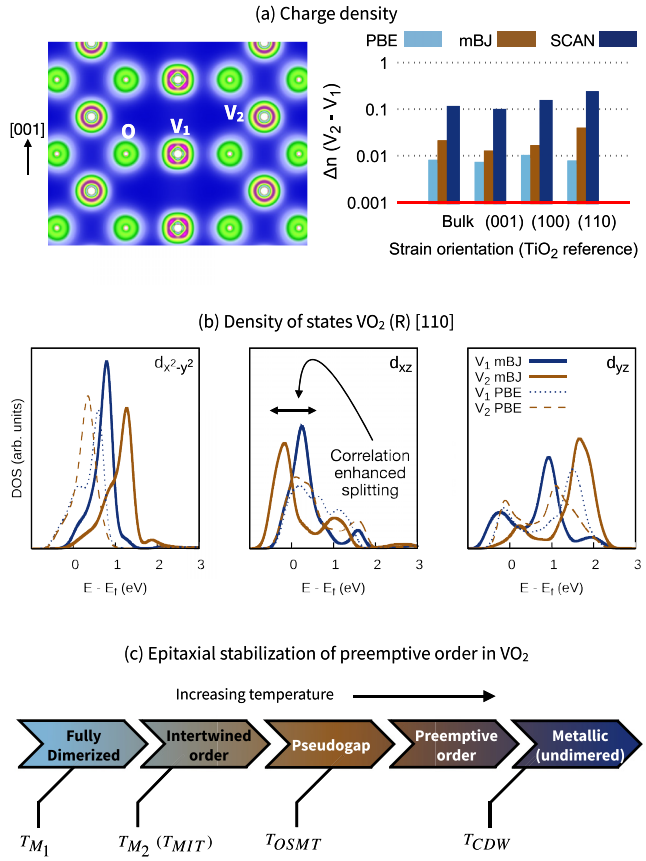

FIG. 3. (a) The charge density map shows density differentiation (mBJ level) and the bar plot shows the occupation difference between the two vanadium sites averaged over different volume conservation conditions. Nonlocal correlations enhance the difference, as do (100) and (110) growth conditions, demonstrating the Mott condition can be engineered by strain. (b) The low-lying vanadium d manifold is split in the strained case by nonlocal correlations (mBJ). The PBE result for bulk rutile VO_2 is shown in grey, where even in the presence of lattice symmetry breaking this is the negligible difference between V_1 and V_2 at the Fermi energy. (c) A proposed phase diagram of VO_2 is shown with preemptive charge ordering occurring before the Peierls transition where charge/orbital ordering is accessed through epitaxial stabilization.

electron correlation are important for the MIT mechanism. In the metallic rutile phase, although the structural changes due to strain have large effects on the electronic properties, this is not sufficient to satisfy the Mott criterion and induce a Mott transition. Nevertheless, electron-electron interactions are still very important and the emergence of charge order in the phase diagram of VO_2 films discovered here echoes the charge density wave states observed in various correlated materials including high-temperature cuprate superconductors [66–70] and transition metal dichalcogenides [71]. It was shown that bulk VO_2 has a charge density wave (CDW) instability exhibited in the momentum density distribution function [72], but it is not strong enough to induce a CDW order. Moreover, we find that the phases observed in VO_2 thin films can be nicely understood as intertwined orders [Fig. 3(c)] between the electronic and structural orders, resembling the phase diagram of the pseudogap in cuprates [73]. In descending from the high-temperature phase, the charge order emerges as a preemptive order, followed by an orbital selective Mott state (OSMT). As the temperature is further lowered to the metal-to-insulator transition temperature T_{MIT}, the electronic CDW/OSMT order is further intertwined with the partial Peierls instability of the M_2 structure and eventually vanishes in the M_1 structure with full dimerization. The existence of the CDW in the M_2 phase was suggested in previous work as well [74]. Our work indicates that strain-engineered, thin-film VO_2 is indeed a strongly correlated system whose correlation can be modulated.

V. CONCLUSION

By interrogating the role of nonlocal correlations in epitaxially strained VO_2 with first-principles plus experimental probes, we find emergent charge order deep in the metallic phase. The existence of nondegenerate vanadium positions induced by strain and enhanced by correlation attests to the importance of Mott physics in the complete phase diagram of thin-film VO_2. Although rutile VO_2 under the largest strain enabled by a TiO_2 substrate cannot become a canonical Mott insulator, electron-electron interactions still result in novel electronic states such as orbital selective Mott states and charge order, hallmarks of the strongly correlated system. Exciting future applications of the VO_2 transition rest on whether or not there exists a fast electronic transition with less reliance on structural transitions, and our work quantifies the strain effects in epitaxially grown thin films. The [001] growth orientation is most bulk-like based on occupancy of the d-manifold and absorption lines, while the [001] and [110] begin to show enhanced correlation effects and spectral features. All of these aspects could have an important impact on designing next-generation memristors utilizing the metal-to-insulator transition of quantum materials.

ACKNOWLEDGMENTS

This work was supported by the Air Force Office of Scientific Research Multi-Disciplinary Research Initiative (MURI) entitled, Cross-Disciplinary Electronic-Ionic Research Enabling Biologically Realistic Autonomous Learning (CEREBRAL), under Award No. FA9550-18-1-0024 administered by Dr. Ali Sayir. We acknowledge Diamond Light Source for time on Beamline I09 under Proposals SI25355 and SI13812 for XAS measurements. For the film synthesis we acknowledge support from the National Science Foundation [Platform for the Accelerated Realization, Analysis, and Discovery of Interface Materials (PARADIM)] under Cooperative Agreement No. DMR-1539918. Substrate preparation was performed, in part, at the Cornell NanoScale Facility, a member of the National Nanotechnology Coordinated Infrastructure (NNCI), which is supported by the National Science Foundation (Grant No. ECCS-1542081). We acknowledge Drs. Tien-Lin Lee and Nicholas Quackenbush for assistance with the XAS measurements at beamline I09 Diamond Light Source.

[1] S. Acharya, C. Weber, E. Plekhanov, D. Pashov, A. Taraphder, and M. Van Schilfgaarde, Phys. Rev. X **8**, 021038 (2018).

[2] M. Yang, Y. Yang, B. Hong, L. Wang, K. Hu, Y. Dong, H. Xu, H. Huang, J. Zhao, H. Chen, L. Song, H. Ju, J. Zhu, J. Bao, X. Li, Y. Gu, T. Yang, X. Gao, Z. Luo, and C. Gao, Sci. Rep. **6**, 23119 (2016).

[3] Y. Kalcheim, N. Butakov, N. M. Vargas, M.-H. Lee, J. del Valle, J. Trastoy, P. Salev, J. Schuller, and I. K. Schuller, Phys. Rev. Lett. **122**, 057601 (2019).

[4] Z. Shao, X. Cao, H. Luo, and P. Jin, NPG Asia Materials **10**, 581 (2018).

[5] Z. Yang, C. Ko, and S. Ramanathan, Annu. Rev. Mater. Res. **41**, 337 (2011).

[6] M. Yamamoto, R. Nouchi, T. Kanki, A. N. Hattori, K. Watanabe, T. Taniguchi, K. Ueno, and H. Tanaka, ACS Appl. Mater. Interfaces **11**, 3224 (2019).

[7] J. Lappalainen, J. Mizsei, and M. Huotari, J. Appl. Phys. **125**, 044501 (2019).

[8] W. Yi, K. K. Tsang, S. K. Lam, X. Bai, J. A. Crowell, and E. A. Flores, Nat. Commun. **9**, 4661 (2018).

[9] A. Rana, C. Li, G. Koster, and H. Hilgenkamp, Sci. Rep. **10**, 1 (2020).

[10] V. Eyert, Ann. Phys. (Leipzig) **11**, 650 (2002)

[11] Z. Hiroi, Solid State Chem. **43**, 47 (2015)

[12] R. Rana, J. M. Klopf, J. Grenzer, H. Schneider, M. Helm, and A. Pashkin, Phys. Rev. B **99**, 041102(R) (2019).

[13] M. J. Wahila, G. Paez, C. N. Singh, A. Regoutz, S. Sallis, M. J. Zuba, J. Rana, M. B. Tellekamp, J. E. Boschker, T. Markurt, J. E. N. Swallow, L. A. H. Jones, T. D. Veal, W. Yang, T.-L. Lee, F. Rodolakis, J. T. Sadowski, D. Prendergast, W.-C. Lee, W. A. Doolittle, and L. F. J. Piper, Phys. Rev. Materials **3**, 074602 (2019).

[14] D. B. Rogers, R. D. Shannon, A. W. Sleight, and J. L. Gillson, Inorg. Chem. **8**, 841 (1969).

[15] M. Imada, A. Fujimori, and Y. Tokura, Rev. Mod. Phys. **70**, 1039 (1998).

[16] R. M. Wentzcovitch, W. W. Schulz, and P. B. Allen, Phys. Rev. Lett. **72**, 3389 (1994).

[17] J. M. Booth and P. S. Casey, Phys. Rev. Lett. **103**, 086402 (2009).

[18] H.-T. Kim, Y. W. Lee, B.-J. Kim, B.-G. Chae, S. J. Yun, K.-Y. Kang, K.-J. Han, K.-J. Yee, and Y.-S. Lim, Phys. Rev. Lett. **97**, 266401 (2006).

[19] M. M. Qazilbash, M. Brehm, B.-G. Chae, P.-C. Ho, G. O. Andreev, B.-J. Kim, S. J. Yun, A. Balatsky, M. Maple, F. Keilmann, H.-T. Kim, and D. N. Basov, Science **318**, 1750 (2007).

[20] M. M. Qazilbash, A. A. Schafgans, K. S. Burch, S. J. Yun, B. G. Chae, B. J. Kim, H. T. Kim, and D. N. Basov, Phys. Rev. B **77**, 115121 (2008).

[21] S. Lee, K. Hippalgaonkar, F. Yang, J. Hong, C. Ko, J. Suh, K. Liu, K. Wang, J. J. Urban, X. Zhang, C. Damessean, A. Hartnoll, O. Delaire, and J. Wu, Science **355**, 371 (2017).

[22] D. Lee, B. Chung, Y. Shi, G.-Y. Kim, N. Campbell, F. Xue, K. Song, S.-Y. Choi, J. Podkaminer, T. Kim, P. J. Ryan, J.-W. Kim, T. R. Paudel, J.-H. Kang, J. W. Spinuzzi, D. A. Tenne, E. Y. Tsymbal, M. S. Rzchowski, L. Q. Chen, J. Lee, and C. B. Eom, Science **362**, 1037 (2018).

[23] T. Lin and Y. Zhang, Vacuum **163**, 338 (2019).

[24] I. Kylänpää, Y. Luo, O. Heinonen, P. R. C. Kent, and J. T. Krogel, Phys. Rev. B **99**, 075154 (2019).

[25] M. W. Haverkort, Z. Hu, A. Tanaka, W. Reichelt, S. V. Streltsov, M. A. Korotin, V. I. Anisimov, H. H. Hsieh, H.-J. Lin, C. T. Chen, D. I. Khomskii, and L. H. Tjeng, Phys. Rev. Lett. **95**, 196404 (2005).

[26] T. C. Koethe, Z. Hu, M. W. Haverkort, C. Schüßler-Langeheine, F. Venturini, N. B. Brookes, O. Tjernberg, W. Reichelt, H. H. Hsieh, H.-J. Lin, C. T. Chen, and L. H. Tjeng, Phys. Rev. Lett. **97**, 116402 (2006).

[27] S. Biermann, A. Poteryaev, A. I. Lichtenstein, and A. Georges, Phys. Rev. Lett. **94**, 026404 (2005).

[28] C. Weber, D. D. O'Regan, N. D. M. Hine, M. C. Payne, G. Kotliar, and P. B. Littlewood, Phys. Rev. Lett. **108**, 256402 (2012).

[29] T. L. Cocker, L. V. Titova, S. Fourmaux, G. Holloway, H.-C. Bandulet, D. Brassard, J.-C. Kieffer, M. A. El Khakani, and F. A. Hegmann, Phys. Rev. B **85**, 155120 (2012).

[30] S. Kim, K. Kim, C.-J. Kang, and B. I. Min, Phys. Rev. B **87**, 195106 (2013).

[31] W. H. Brito, M. C. O. Aguiar, K. Haule, and G. Kotliar, Phys. Rev. Lett. **117**, 056402 (2016).

[32] J. del Valle, P. Salev, Y. Kalcheim, and I. K. Schuller, Sci. Rep. **10**, 4292 (2020)

[33] Y. Kalcheim, A. Camjayi, J. del Valle, P. Salev, M. Rozenberg, and I. K. Schuller, Nat. Commun. **11**, 2985 (2020).

[34] T. Driscoll, H.-T. Kim, B.-G. Chae, M. Di Ventra, and D. Basov, Appl. Phys. Lett. **95**, 043503 (2009).

[35] D. B. Strukov, G. S. Snider, D. R. Stewart, and R. S. Williams, Nature (London) **453**, 80 (2008).

[36] J. Von Neumann, IEEE Annals of the History of Computing **15**, 27 (1993).

[37] J. del Valle, P. Salev, F. Tesler, N. M. Vargas, Y. Kalcheim, P. Wang, J. Trastoy, M.-H. Lee, G. Kassabian, J. G. Ramírez, M. J. Rozenberg, and I. K. Schuller, Nature (London) **569**, 388 (2019).

[38] J. Laverock, A. R. H. Preston, D. Newby, K. E. Smith, S. Sallis, L. F. J. Piper, S. Kittiwatanakul, J. W. Lu, S. A. Wolf, M. Leandersson, and T. Balasubramanian, Phys. Rev. B **86**, 195124 (2012).

[39] H. Paik, J. a. Moyer, T. Spila, J. W. Tashman, J. a. Mundy, E. Freeman, N. Shukla, J. M. Lapano, R. Engel-Herbert, W. Zander, J. Schubert, D. a. Muller, S. Datta, P. Schiffer, and D. G. Schlom, Appl. Phys. Lett. **107**, 163101 (2015).

[40] N. F. Quackenbush, H. Paik, J. C. Woicik, D. A. Arena, D. G. Schlom, and L. F. J. Piper, Materials **8**, 5452 (2015).

[41] S. Mukherjee, N. F. Quackenbush, H. Paik, C. Schlueter, T.-L. Lee, D. G. Schlom, L. F. J. Piper, and W.-C. Lee, Phys. Rev. B **93**, 241110(R) (2016).

[42] N. F. Quackenbush, H. Paik, M. J. Wahila, S. Sallis, M. E. Holtz, X. Huang, A. Ganose, B. J. Morgan, D. O. Scanlon, Y. Gu, F. Xue, L.-Q. Chen, G. E. Sterbinsky, C. Schlueter, T.-L. Lee, J. C. Woicik, J.-H. Guo, J. D. Brock, D. A. Muller, D. A. Arena, D. G. Schlom, and L. F. J. Piper, Phys. Rev. B **94**, 085105 (2016).

[43] W.-C. Lee, M. J. Wahila, S. Mukherjee, C. N. Singh, T. Eustance, A. Regoutz, H. Paik, J. E. Boschker, F. Rodolakis, T.-L. Lee, D. G. Schlom, and L. F. J. Piper, J. Appl. Phys. **125**, 082539 (2019).

[44] A. D'Elia, S. Rezvani, A. Cossaro, M. Stredansky, C. Grazioli, B. W. Li, C. Zou, M. Coreno, and A. Marcelli, J. Supercond. Nov Magn. **33**, 2383 (2020).
[45] B. Lazarovits, K. Kim, K. Haule, and G. Kotliar, Phys. Rev. B **81**, 115117 (2010).
[46] S. Niitaka, H. Ohsumi, K. Sugimoto, S. Lee, Y. Oshima, K. Kato, D. Hashizume, T. Arima, M. Takata, and H. Takagi, Phys. Rev. Lett. **111**, 267201 (2013).
[47] S. Guan, A. Rougier, M. R. Suchomel, N. Penin, K. Bodiang, and M. Gaudon, Dalton Transactions **48**, 9260 (2019).
[48] A. Zylbersztejn and N. F. Mott, Phys. Rev. B **11**, 4383 (1975).
[49] Z. Zhu and U. Schwingenschlögl, Phys. Rev. B **86**, 075149 (2012).
[50] I. Kylänpää, J. Balachandran, P. Ganesh, O. Heinonen, P. R. C. Kent, and J. T. Krogel, Phys. Rev. Materials **1**, 065408 (2017).
[51] A. S. Belozerov, M. A. Korotin, V. I. Anisimov, and A. I. Poteryaev, Phys. Rev. B **85**, 045109 (2012).
[52] M. C. Sánchez, G. Subías, J. García, and J. Blasco, Phys. Rev. Lett. **90**, 045503 (2003).
[53] M. Medarde, C. Dallera, M. Grioni, B. Delley, F. Vernay, J. Mesot, M. Sikora, J. A. Alonso, and M. J. Martínez-Lope, Phys. Rev. B **80**, 245105 (2009).
[54] K. Momma and F. Izumi, J. Appl. Crystallogr. **44**, 1272 (2011).
[55] M. Sambi, M. Della Negra, and G. Granozzi, Thin Solid Films **400**, 26 (2001).
[56] A. O'Hara and A. A. Demkov, Phys. Rev. B **91**, 094305 (2015).
[57] P. Blaha, K. Schwarz, G. K. H. Madsen, D. Kvasnicka, and J. Luitz, *WIEN2K, An Augmented Plane Wave + Local Orbitals Program for Calculating Crystal Properties*, Karlheinz Schwarz, Techn. Universität Wien, Austria, 3-9501031-1-2.
[58] J. P. Perdew, K. Burke, and M. Ernzerhof, Phys. Rev. Lett. **77**, 3865 (1996).
[59] D. Koller, F. Tran, and P. Blaha, Phys. Rev. B **85**, 155109 (2012).
[60] J. Sun, A. Ruzsinszky, and J. P. Perdew, Phys. Rev. Lett. **115**, 036402 (2015).
[61] Y. Quan, V. Pardo, and W. E. Pickett, Phys. Rev. Lett. **109**, 216401 (2012).
[62] R. S. Mulliken, J. Chem. Phys. **23**, 1833 (1955).
[63] R. F. Bader, Acc. Chem. Res. **18**, 9 (1985).
[64] F. L. Hirshfeld, Theor. Chim. Acta **44**, 129 (1977).
[65] D. J. Singh and L. Nordstrom, *Planewaves, Pseudopotentials, and the LAPW Method* (Springer Science & Business Media, New York, 2006).
[66] W. Atkinson, A. P. Kampf, and S. Bulut, New J. Phys. **17**, 013025 (2015).
[67] M. Vojta and S. Sachdev, Phys. Rev. Lett. **83**, 3916 (1999).
[68] A. Damascelli, Z. Hussain, and Z.-X. Shen, Rev. Mod. Phys. **75**, 473 (2003).
[69] S. A. Kivelson, I. P. Bindloss, E. Fradkin, V. Oganesyan, J. M. Tranquada, A. Kapitulnik, and C. Howald, Rev. Mod. Phys. **75**, 1201 (2003).
[70] P. A. Lee, N. Nagaosa, and X.-G. Wen, Rev. Mod. Phys. **78**, 17 (2006).
[71] K. Rossnagel, J. Phys.: Condens. Matter **23**, 213001 (2011).
[72] P. Ganesh, F. Lechermann, I. Kylänpää, J. T. Krogel, P. R. C. Kent, and O. Heinonen, Phys. Rev. B **101**, 155129 (2020).
[73] E. Fradkin, S. A. Kivelson, and J. M. Tranquada, Rev. Mod. Phys. **87**, 457 (2015).
[74] T. V. Slusar, J.-C. Cho, H.-R. Lee, J.-W. Kim, S. Jo Yoo, J.-Y. Bigot, K.-JuYee, and H.-T. Kim, Sci. Rep. **7**, 16038 (2017).